S92944

A FAST CODE FOR JUPITER ATMOSPHERIC ENTRY

Michael E. Tauber*, Thermosciences Institute, Moffett Field, CA
Paul Wercinski+, NASA-Ames Research Center, Moffett Field, CA
Lily Yang#, Raytheon Corp., Lanham, MD
Yih-Kanq Chen§, NASA-Ames Research Center, Moffett Field, CA

ABSTRACT

A fast code was developed to calculate the forebody heating environment and heat shielding that is required for Jupiter atmospheric entry probes. A carbon phenolic heat shield material was assumed and, since computational effiency was a major goal, analytic expressions were used, primarily, to calculate the heating, ablation and the required insulation. The code was verified by comparison with flight measurements from the Galileo probe's entry; the calculation required 3.5 sec of CPU time on a work station. The computed surface recessions from ablation were compared with the flight values at six body stations. The average, absolute, predicted difference in the recession was 12.5% too high. The forebody's mass loss was overpredicted by 5.5% and the heat shield mass was calculated to be 15% less than the probe's actual heat shield. However, the calculated heat shield mass did not include contingencies for the various uncertainties that must be considered in the design of probes. Therefore, the agreement with the Galileo probe's values was considered satisfactory, especially in view of the code's fast running time and the methods' approximations.

NOMENCLATURE

A	base area, m^2
C_D	drag coefficient
m	mass, kg
p	pressure, atm
q	heating rate, kW/cm^2
q_R	radiative heating rate, kW/cm^2

---

* Sr. Research Scientist, Assoc. Fellow AIAA
\+ Reacting Flow Environments Branch Chief
\# Sr. Programmer/Analyst
§ Research Scientist

q_{AR} radiative heating rate assuming adiabatic flow, kW/cm^2
R radius measured from body centerline, m
S distance measured along body surface, m
t time from entry at 450 km altitude, sec
V flight velocity, m/sec
Γ Goulard number (see Eq. 2)
ρ ambient atmospheric density, kg/m^3

INTRODUCTION

The strong gravitational attraction of Jupiter on probes approaching the planet results in very high atmospheric entry velocities. The values relative to the rotating atmosphere can vary from about 47 to 60 km/sec, depending on the flight path angle and the latitude of the entry. Therefore, the peak heating rates and heat shield mass fractions exceed those for any other atmospheric entry. For example, the Galileo probe's heat shield mass fraction was about 48%, of which over 42% was devoted to the forebody. Although the Galileo probe's mission was very successful, many more scientific questions about the Jovian atmosphere remain to be answered and additional probe missions are being planned.

A number of large and complex computer codes were developed in the period between approximately 1970 and 1980 that were used to determine the Galileo probe's entry heating environment (Refs. 1-3). The results from the codes were used to calculate the thermal protection system (TPS) required to shield the probe from the severe entry heating. Chemical reactions, ablation and one-dimensional thermal conduction computations were combined to calculate the heat shield material thickness distribution over the body so that a specified temperature limit would be observed at the bondline between the heat shield and the structure (Ref. 4). These codes were sophisticated and complex; a complete solution of the heating distribution over the ablating forebody, at one point in the trajectory, could take on the order of one hour of computer time. However, once the probe's external configuration at entry was defined, the heating and TPS thickness would only have to be calculated once for each hypothesized atmospheric composition and trajectory.

Recent developments in microelectronics should make it possible to build smaller and much less expensive probes than Galileo. Therefore, it was desirable to develop a code that could compute the forebody entry heating environments and TPS masses for performing parametric probe sizing studies. Such a code would have to run much faster than the ones used to design the Galileo probe, although some precision might have to be sacrificed for speed. The Jupiter

Atmospheric Entry (JAE) code was developed to meet the requirements of being fast and enabling both the forebody's shape and size to be varied parametrically.

ANALYSIS

The formulations that were used to calculate the forebody heating and ablation follow the methods described in Ref. 5. To reduce computational complexity and time, analytic expressions were developed and used for calculating the shock shapes, flow field, heating, ablation, etc., although iteration was required frequently. Also, advantage was taken of the results from the more rigorous flow field and heating calculations that were published, or presented, subsequently to Ref. 5. The atmospheric structure and composition that was measured by the Galileo probe was used, with some small variation, as will be discussed later. An existing trajectory code was employed and the ballistic coefficient was updated at each time step in the calculation. The probe's body geometry was assumed to be similar to Galileo, see Fig. 1, consisting of a blunt-nosed conical shape of arbitrary nose and base radius and cone angles up to about 65 deg, at zero angle of attack. (The cone angle limitation is imposed by the assumption that the shock on the conical frustum is straight and the inviscid shock layer angular thickness is much less than the cone angle.) The TPS material was limited to carbon-phenolic since it was used successfully on the Galileo probe's forebody and some very high heating rate ground-facility test data were available in the open literature (Ref. 6 and 7).

Trajectory

The trajectory code that was used employs an Adams-Moulton predictor-corrector method to solve the equations of motion. The code includes the effects of planetary rotation and oblateness; both of these properties have a major influence on the trajectory, especially at Jupiter which has a very large rotational rate and oblateness. The atmospheric structure and composition that was derived from the Galileo entry probe's measurements (Ref. 8) was incorporated into the trajectory calculation. The nominal volumetric atmospheric composition was found to have been 86.2% hydrogen, 13.6% helium and trace amounts of methane, ammonia, etc., yielding a molecular weight of 2.35. The trajectory calculation was begun at an altitude of 450 km, where the datum is the altitude at which the pressure is one bar; 0.1 sec time intervals were used in the computation. Since the massive ablation experienced by probes during Jupiter atmospheric passage reduced the body's mass and size and changed the drag coefficient, the ballistic coefficient (m/C_DA) was updated at each time step. The mass loss was computed only for the forebody, since the afterbody flow field and the interaction of the heating and ablation in that region would have

made the calculation excessive complex and time consuming. In addition, the afterbody's mass loss was a small fraction of the total value. For example, the forebody's mass loss on the Galileo probe was almost 25% of the entry mass; in contrast the afterbody's mass loss was estimated to have been 2.5%, plus or minus 1% (Ref. 9).

Flow Field

The equilibrium thermodynamic and transport properties of the atmospheric gases at high temperatures were taken from Ref. 5, where an ambient composition of 85% hydrogen and 15% helium had been assumed. (The thermodynamic properties were checked by calculating equilibrium values (Ref. 10) for a composition of 86% hydrogen and 14% helium. At the same enthalpy and pressure, the temperature differences between the two compositions varied from less than 1% to a maximum of about 1.5%. This difference was considered to have a negligibly effect on the present analysis.) The thermodynamic equilibrium temperatures behind a shock in the Jovian atmosphere are shown in Fig. 2 as a function of the velocity normal to the shock wave and for pressures from 0.1 to 100. atm. Although shock layer temperatures in the vicinity of 15,000 K occur during entry, the values are much less than in air at comparable pressures and flight velocities. For example, at a post-shock pressure of one atmosphere and a normal shock velocity of about 44 km/sec, the temperature at Jupiter is 15,000 K; the same post-shock conditions would occur in air at a normal shock velocity of about 15 km/sec. The large difference in temperatures between the two gases results primarily from the much lower molecular weight and, therefore, the much higher specific heat of the predominantly hydrogen Jovian atmosphere, compared to air. It is this difference in the temperatures between the two gases that enables the design of probes that can survive the nearly 50 km/sec entries into Jupiter, using current TPS technology.

The intensity of the radiative emission from an isothermal slab of shock layer gas of a specified thickness, to account for self-absorption, was taken from Ref. 5, again for a 85% hydrogen and 15% helium composition. The intensities used in Ref. 5 were calculated and tabulated as a function of the velocity normal to the shock for pressures from 0.1 to 100. atm. An example is shown in Fig. 3, where the intensity of the emission from a 1. cm thick isothermal slab of gas is plotted as a function of the normal velocity for shock-layer pressures of 1. and 10. atm. Note the very large radiative intensities; for example, at a velocity of 40 km/sec and 10. atm of pressure, the value is almost 100. kW/cm^2. In the JAE code, the shock layer was assumed to be in thermochemical equilibrium since the pressures were large (typically 1. to 10. atm) at those times in the trajectories when heating and ablation were severe.

The shock wave shape about the assumed probe configuration was analyzed in three parts; these consisted of the blunt-nosed spherical section, the cone frustum and the narrow flat ring that forms the outer edge of the body. On the blunt nose, the shock stand-off distance was calculated as a function of the local density ratio across the shock wave and the angular position from the stagnation point. On the cone frustum, the shock was assumed to be straight and, therefore, a function only of cone angle, ablation boundary layer thickness and density ratio across the shock wave. Assuming that the shock on the cone frustum is straight is not excessively restrictive. It requires that the body's nose radius be significantly less than the base radius and that the cone angle not be so large that the inviscid shock layer flow becomes subsonic on the cone frustum. When the inviscid flow on the cone becomes subsonic, the shock wave ceases to be straight (Ref. 11) and the shock layer becomes much thicker and hotter. Therefore, large nose radii and large cone angles (on the order of, or greater than approximately 65 deg) result in much more intense radiative heating, and such configurations should be avoided at any rate. Flow conditions on the flat ring were computed by assuming that the inviscid flow expanded isentropically from the cone frustum. For the purpose of computing the shock shape and the inviscid flow field (only), the non-adiabatic effect resulting from radiative emission (that altered the temperature and density downstream of the shock) was neglected. However, the energy loss from radiation that caused the inviscid flow to be non-adiabatic was accounted for in the heating calculations.

Heating Environment

The high entry velocities that are experienced at Jupiter result in very large heating rates. The dominant source of heating is shock-layer radiation, although turbulent boundary layer convection also contributes significantly. In fact, the turbulent boundary layer heating can become comparable to the radiative component on the cone frustum of bodies having "moderate" cone angles, such as the Galileo probe, as will be shown. In contrast to the turbulent boundary layer, the laminar boundary layer convective heating contribution is a small fraction of the total heating, usually, since it is blocked much more effectively by the ablation product gases.

The radiative heating is computed assuming that the transport is one-dimensional, i.e. normal to the shock wave toward the body, on the spherically blunted nose cap, the conical forebody and the narrow flat ring. This assumptions has been shown to be a good approximation in the stagnation region of blunt bodies (Ref. 12) for shock layers that are thin compared to the nose radius. On the cone frustum, the assumption of one-dimensional transport may be less valid than in the stagnation region. However, the one-dimensional radiative transport assumption is used here nonetheless (and in most other

codes), since more precise methods can increase code complexity and computing time by orders of magnitude. The radiation was computed using tables of intensity that were functions of the velocity component normal to the shock wave and the shock layer pressure and the inviscid shock layer thickness to account for self-absorption (Ref. 5). The resulting values were then corrected for nonadiabatic flow effects (sometimes referred to as radiative cooling), by using the following expression for the hydrogen-helium gas mixture given in Ref. 5,

$$q_R/q_{AR} = 1/(1+3\Gamma^{0.7}) \qquad (1)$$

and

$$\Gamma = 2q_{AR}/0.5\rho V^3 \qquad (2)$$

where Γ is the Goulard number and the heating rate, q, is in W/m^2. (Note that Eq. 1 differs from Goulard's original expression (Ref. 13) since Γ is multiplied by a constant and raised to the 0.7 power. These are empirical modifications to Goulard's original expression which was derived for $\Gamma \ll 1$ and had values of 1. for both the constant and exponent. However, it can be shown that with appropriate empirically derived values of the constant and exponent, Goulard's expression can yield good results for air radiation, for example, for values as large as $\Gamma = 1$.)

The absorption of radiation by the carbon phenolic ablation vapors, in a laminar boundary layer, was correlated as a function of the total (radiation plus convection) non-ablating wall heat transfer rate (Ref. 1) and extended in Ref. 14. Although the correlation's of Ref. 1 and 14 were limited to the stagnation point, the results were applied over the entire body, for lack of more applicable calculations. When the boundary layer was fully turbulent, it was assumed that radiation penetrated the ablation layer without attenuation, based on the calculated results shown in Ref. 2. For the transitional boundary layer, it was assumed that the fraction of radiation that was blocked varied linearly from the laminar value to the zero (unblocked) turbulent value.

The convective heating was calculated over the body for laminar, transitional and turbulent boundary layers and, in each case, accounting for blockage by ablation vapors. On the blunt nose and the cone frustum, the non-ablating heating rates were formulated as functions of the flight conditions, the local surface slopes, body location and wall enthalpy. The resulting expressions greatly speeded the computation. The non-ablating laminar convective stagnation point heating was based on the results of Refs. 15 and 16. In the formulations, modifications were made, when necessary, using the thermodynamic and transport properties for the Jovian atmospheric gas composition. The convective heating distribution off the stagnation point on the blunt nose was based on the local surface slope. On the cone frustum, the nonablating laminar and turbulent heating was calculated following the

procedures that were described in Refs. 17 and 18, but modified for the proper gas composition. On the narrow flat ring, the convective heating expressions were written as a function of the surface pressure. The surface pressure was found by assuming the flow expanded isentropically from the cone to the flat surface. Since the presence of the fairly thick ablation product boundary layer was ignored in computing the flow expansion, the pressures, and the convective heating on the ring was underestimated. (The heating of the ring's surface is dominated by radiation and, furthermore, its area is a small fraction of the entire forebody's surface area. Therefore, improving the present calculation of the pressure has been postponed until a more accurate, but also more complex procedure, can be implemented.)

The transition of the boundary layer from laminar to turbulent flow is the most complex phenomenon that affects the calculation of the entry heating. It is difficult to predict the location of transition on entry vehicles with nonablating surfaces (for example, see Refs. 17 and 19); the complexity is greatly compounded when massive ablation occurs (Ref. 17). In most of the computations that were used to design the Galileo probe (Refs. 1-3), transition locations were assumed, or local Reynolds numbers based on momentum thickness were employed; in both cases, transition began near the stagnation point. In Ref. 5, a computationally simpler transition criterion based on boundary layer edge length Reynolds number was used and the value was varied parametrically to study its effect. A boundary layer edge length Reynolds number for the beginning of transition was made an input in the JAE code; however, because of its uncertainty and strong influence on heating, an approximate value for the beginning of transition Reynolds number was backed-out from the Galileo surface recession data that will be discussed later. The length of the transitional flow region was formulated as a function of the distance of the preceding laminar boundary layer. In the transitional zone, the convective heating in the presence of ablation was assumed to vary linearly with distance along the surface, from the laminar to the turbulent value. However, after including the radiative heating contribution, the heating distribution in the transitional zone was no longer linear. The linear variation of convective heating in the transitional region was used because it was easily implemented and computationally efficient, despite the fact that the gradients that resulted at the beginning and end of transition were excessively steep (Ref. 20).

The formulation for the blockage of both laminar and turbulent convective heating was based on that presented in Ref. 17; this expression consisted of a quadratic equation that was a function of the mass injection, i.e. blowing rate. (It can be shown (Ref. 21) that the quadratic equation can be derived from the more widely used exponential expression, but is used here because it can be solved more quickly than the exponential one.) However, the blowing rate

calculation was coupled to include the effect of radiative heating. The coefficients of the quadratic equation were modified to account for reactions of the Jovian atmospheric shock layer gases. The effect of chemical reactions with the ablation products was not considered explicitly, but were accounted for in the ablation material response. In addition, the coefficients were functions of the pressure gradient on the surface and differ for laminar and turbulent boundary layers. As would be expected, when strong radiative heating occurred most, or all, of the laminar convective heating was blocked. In contrast, turbulent boundary layer convection was a significant fraction of the total heating rate, even when strong radiation produced large mass injection rates.

Ablation Material Response

The response of the carbon-phenolic ablation material to the heating was modeled as surface sublimation (Refs. 6, 7 and 22) and reradiation. Omitting the conduction term was justified on the basis that the high heating rates experienced during Jovian entry caused rapid surface recession, as will be shown. Therefore, only a small fraction of the energy was conducted into the virgin material during the high heating period; omitting the conduction term resulted in a major simplification of the code and saving of computational time. The thickness of virgin carbon-phenolic that was needed for insulation was determined from empirical expressions that were derived from calculations using the Fully Implicit Ablation and Thermal Response Program (FIAT), Ref. 4. The FIAT calculations were made assuming a bond-line temperature of 517 K and that the heat shield would separate at a speed of 0.6 km/sec, or approximately Mach 0.8. The heat capacity of the structure was accounted for by assuming the same aluminum alloy as that used on the Galileo probe and scaling the thickness as a function of the maximum stagnation pressure, which is directly proportional to the maximum deceleration.

Spallation of the heat shield material was formulated in the JAE code using the experimentally derived model of Lundell (Ref. 23) that was employed in the design of the Galileo probe. The heating source in the experiment was the monochromatic beam from a high-power carbon dioxide laser. Two different spallation models were presented in Ref. 23. One model was applicable to the chopped-molded carbon-phenolic that was used for the nose cap of the Galileo probe and the second for the 30 deg tape-wrapped material on the cone frustum. Both materials employed 24 layers of carbon cloth per centimeter of thickness and have the same virgin bulk density of 1450 kg/m^3. Threshold heating rates, below which spallation was not observed, were listed in Ref. 23 as 14.5 and 8.5 kW/cm^2 for the chopped-molded and tape-wrapped forms of carbon-phenolic, respectively.

Code Output

The above described analysis procedure was used to calculate the atmospheric trajectory, the heating of the forebody, surface recessions from ablation and spallation, and forebody mass loss as a function of time. In addition, the residual thickness and mass of carbon phenolic insulation that was required was printed at the end. The computation was performed at 0.1 sec intervals and the ballistic coefficient was updated at each time step. Approximately 75 points were located initially on a typical forebody configuration such as the Galileo probe, including the ring forming the outer edge. (On the blunt nose, the heating and ablation was calculated at 1. deg intervals; however, the number of points changed since ablation altered the nose shape.) At selected time steps, the output consisted of convective and radiative heating, both with and without ablation, the heat load integrated over the body, the surface recessions at selected body locations, the mass loss from spallation and the total mass loss integrated over the entire forebody. The ballistic coefficient was printed, also. Next, computations from the JAE code will be compared with the Galileo probe data.

CALCULATIONS FOR GALILEO PROBE ENTRY

The JAE code was used to reproduce the Galileo probe's entry and the calculated surface recessions were compared with the values from the flight data. The initial conditions that were used for the trajectory were, in inertial reference system coordinates, at an alttitue of 450 km:
velocity = 59.92 km/sec, flight path angle = -6.64 deg, azimuth angle = 90 deg, latitude = 6.52 deg and zero angle of attack.
The resulting entry velocity relative to the rotating atmosphere was calculated to be 47.37 km/sec. The variation of relative velocity with altitude is shown in Fig. 4. Note that most of the deceleration, and therefore heating, occurs at altitudes from about 200 km to 70 km.

The major uncertainty in the heating calculations was the choice of transition Reynolds number, as previously stated. Initially, values ranging from 50,000 to 200,000 were tried and large differences in surface recessions and forebody mass loss were found. Finally, the Galileo probe data (Ref. 9) was used to back-out a value of 120,000 and this was used in the results presented here. The heating rates, surface recessions, etc., were computed in a single run on a work station in 3.5 sec of CPU time.

The heating rate with ablation is shown as a function of time in Figs. 5. The stagnation point heating rate (Fig. 5a) peaks at about 53 sec at a value of 17 kW/cm^2 and radiation is the dominant source. In contrast, on the cone frustum

(Fig. 5b) near the the centroid of the area at an initial radius, R, of 0.4424 m, the radiative heat load is actually somewhat less than the predominantly turbulent convection. At this body location, boundary layer transition begins at about 43 sec and turbulence is fully established at about 48 sec. The maximum heating rate was calculated to be 10.6 kW/cm^2, again at 53 sec.

Next, the calculated heating rate distributions over the ablating body's surface are illustrated in Figs. 6 at times corresponding to 5 sec before the peak heating rate, at peak heating and 5 sec after peak heating. The ablating surface heating rate at t = 48 sec is shown in Fig. 6a. On the blunt nose, where radiative heating is large and the boundary layer is laminar, convective heating is negligible. Transition begins on the cone frustum. However, the combination of relatively high altitude, i.e. low ambient density, and blockage by massive ablation products from radiative heating, result in convection accounting for about one-third of the heating intensity on the conical surface. At the time of maximum heating, t = 53 sec, (Fig. 6b), transition begins on the blunt nose, just ahead of the junction with the conical surface. Although radiation dominates the heating over much of the surface, the contribution of turbulent convection is becoming larger, especially near the junction. Also evident in Fig. 6b, is the predicted steep increase in the heating caused by transition, in the vicinity of S = 0.2 m, for example. At t = 58 sec, in Fig. 6c, the vehicle has decelerated sufficiently so that only the blunt nose experiences radiative heating, since the temperatures in the conical surface's shock layer are too low for significant radiative emission. In contrast, turbulent convection causes severe heating on the cone frustum, with a predicted peak value of over 8 kW/sq cm. Again, the computed steep heating gradient in the transitional boundary layer region is evident.

Before comparing the surface recessions from the JAE code with the Galileo probe measurements, it is instructive to compare with some values that were computed using the FIAT code. The two body locations that were used consisted of the stagnation point and the approximate centroid of the cone at R = 0.4424 m. The FIAT computation was performed using the convective and radiative heating rates and surface pressures from the JAE code. The stagnation point recession that was predicted by both codes was the same, essentially, differing by only 0.1%. At the point on the cone frustum, FIAT predicted a recession that was 5.2% higher than JAE. Therefore, both codes predicted very similar recessions.

Comparison with Galileo Probe Data

The surface recession histories that were computed using the JAE code were compared to the values measured during entry of the Galileo probe at six body stations (Ref. 9). Only one set of two ablation gages was located on the probe's

nose, 11.2 deg off the stagnation point. The surface recession that was calculated at 12 deg off the stagnation point is compared with the data in Fig. 7a. The agreement is considered good; the final computed recession at the end of ablation is 10.7% higher than the measured value. The next station had a single ablation gage that was located at an initial radius, measured from the body's centerline, of R = 0.2200 m. Results from the computation, at R = 0.2207 m, are shown in Fig. 7b. The calculated recession is very close to the measured value being only 0.4% high. Another, single, ablation gage was located at R = 0.3177 m and the nearest computed station was at R = 0.3157 m. At this body location (Fig. 7c), the recession is poorly predicted; the final value is 32.1% too high. The reason for the excessively high predicted ablation at this station is not obvious. One contributing factor may be the steep gradient of the heating rate, at the fully developed turbulence location, that results from the assumption of a linear variation of heating in the transitional region. Two ablation gages were located at the next downstream station of R = 0.4343 m and the nearest computed station was at 0.4424 m. The surface recessions agree well at this body location (Fig. 7d) with the calculated final value being 9.9% too high. The last two gages on the cone frustum were at R = 0.5497 m and the nearest computational station was at R = 0.5375 m. Again, the final recessions agreed well (Fig. 7e) with the computed value being only 6.9% too low. However, the calculated recessions at 50 and 55 sec were substantially lower than the measured values, indicating that the radiative heating was underpredicted, but this was partially compensated for by reduced blockage of turbulent convection. The last set of two gages was located in the flat ring section, at R = 0.6325 m and the recessions are compared in Fig. 7f. The good agreement at 50 and 55 sec indicates that the radiative heating was well predicted. However, as previously mentioned, the turbulent convection is underpredicted on the ring, resulting in a final calculated recession that is 15.1% too low. The average, absolute, difference between the JAE code computed recessions and the values that were measured at the six body locations during the Galileo probe's entry is 12.5%. Considering the speed of the JAE code and the complexity of computing the severe heating conditions that were experienced by the probe, the above comparisons indicate that the JAE code predicts the surface recessions adequately.

Comparison of Forebody Ablation Mass Losses

Milos (Ref. 9) integrated the surface recession history of the Galileo probe's forebody to yield the mass-loss variation during the entry. The mass-loss history that was computed using the JAE code is compared with that from the Galileo probe in Fig. 8. The JAE values are somewhat low at 50 and 55 sec as is to be expected from the recession comparisons described above. However, the final value is only 5.5% higher than Milos' mean for the Galileo probe and falls at the upper boundary of his uncertainty limits. (In a private communication with D. B.

Kirk of Ref. 8, that author indicated that using a final ablated forebody mass value that is near the upper limit shown in Fig. 8 in the trajectory reconstruction yields the best results when combined with the on-board measurements made during the entry.)

The continous change of the ballistic coefficient that is caused by ablation was included in the trajectory calculation, as was previously discussed. The variation of the Galileo probe's ballistic coefficient with flight velocity is shown in Fig. 9. At entry, the coefficient is 256 kg/m^2 and when ablation ceases, at t = 68 sec and a flight velocity of 12 km/sec, the value has decreased to 222.6 kg/m^2, or by 13%. Ignoring such a large change in the ballistic coefficient leads to significant errors in the calculation of the trajectory.

Comparison of Forebody Heat Shield Masses

Lastly, the forebody heat shield mass that is calculated by the JAE code is compared with that of the Galileo probe. The JAE code predicts a forebody heat shield mass of 121.5 kg for the probe, compared to the actual mass (Ref. 9) of 143 kg, or 15% less than the actual value. However, the calculated value does not include the uncertainties that were considered in the design of the probe's heat shield. Among these were uncertainties in the atmospheric composition and structure, the entry conditions, heating calculations, material response, etc. The heat shield mass that is calculated by the JAE code does not include margins and contingencies to account for various uncertainties that must be added to arrive at a realistic mass.

CONCLUDING REMARKS

The Jupiter atmospheric entry code was developed in response to a need for a analytic methodology that could be used to calculate the heating environment and the forebody thermal protection mass quickly for different forebody geometries. A carbon phenolic heat shield material was assumed and analytic expression were used to calculate the heating, ablation and the insulation requirements for computational efficiency. Only the trajectory calculation employs a finite differencing procedure. The Galileo probe's entry was calculated with the JAE code on a work station in 3.5 sec of CPU time. The calculated surface recessions from ablation were compared with values that were measured during the probe's entry at six body locations. The average, absolute, difference in the recession at the end of ablation that was predicted by the code was 12.5% too high. The entire forebody's mass loss was overpredicted by 5.5%. The forebody's heat shield mass, including insulation, was calculated to be 15% less than the probe's actual heat shield mass. However, the calculated heat shield

mass represented a minimum value that did not include contingencies for the various uncertainties that must be considered in the design of actual probes. Therefore, the code gives satisfactory results for ablation mass loss, ballistic coefficient variation and heat shield mass, and runs very fast. In summary, the JAE code is an efficient and useful tool for parametric studies of Jupiter atmospheric entry probe heat shielding requirements.

ACKNOWLEDGMENTS

This work was supported by NASA Ames Research Center, through contract NAS2-14301 to ELORET. The authors thank Dr. Frank Milos of NASA-Ames for use of the Galileo probe data shown in Figs. 7 and 8.

REFERENCES

1) Moss, J. N., Jones, J. J. and Simmonds, A. L., "Radiative Flux Penetration Through a Blown Shock Layer for Jupiter Entry", AIAA Paper 78-908, May 1978.

2) Moss, J. N. and Kumar, A., "Significance of Turbulence and Transition Location on Radiative Heating with Ablation Injection", AIAA Paper 81-0281, Jan. 1981.

3) Balakrishnan, A. and Nicolet, W. E., "Galileo Probe Forebody Thermal Protection: Benchmark Heating Environment Calculations", AIAA Paper 81-1072, June 1981.

4) Chen, Y.-K. and Milos, F. S., "Ablation and Thermal Response Program for Spacecraft Heatshield Analysis", AIAA Paper 98-0273, Jan. 1998.

5) Tauber, M. E. and Wakefield, R. M., "Heating Environment and Protection During Jupiter Entry", Journal of Spacecraft and Rockets, Vol. 8, No. 6, June 1971, pp.630-636.

6) Park, C., Lundell, J.H., Green, M.J., Winovich, W. and Covington, M.A., "Ablation of Carbonaceous Materials in a Hydrogen-Helium Arcjet Flow", AIAA Journal, Vol. 22, No. 10, October 1984, pp.1491-1498.

7) Howe, J. T., Pitts, W. C. and Lundell, J. T., "Survey of the Supporting Research and Technology for the Thermal Protection of the Galileo Probe", AIAA Paper 81-1068, June 1981.

8) Seiff, A., Kirk, D.B., Knight, T.C.D., Young, R.E., Mihalov, J.D., Schubert, G., Blanchard, R.C. and Atkinson, D., "Thermal Structure of Jupiter's Atmosphere Near the Edge of a 5-micron Hot Spot in the North Equatorial Belt", Journal of Geophysical Research-Planets, Vol. 103, No. E10, Sept. 25, 1998.

9) Milos, F. S., "Galileo Probe Heat Shield Ablation Experiment", Journal of Spacecraft and Rockets, Vol. 34, No. 6, Nov.-Dec. 1997, pp.705-713.

10) Horton, T. E. and Menard, W. A., "A Program for Computing Shock-Tube Gasdynamic Properties", Jet Propulsion Laboratory, Pasadena, CA, Jan. 1969.

11) Hayes, W. D. and Probstein, R., "Hypersonic Flow Theory", Academic Press, New York, N.Y., 1959.

12) Howe, J.T. and Viegas, J.R., "Solutions of the Ionized Radiating Shock Layer, Including Reabsorption and Foreign Species Effects, Stagnation Region Heat Transfer", NASA TR R-159, 1963.

13) Goulard, R., "Preliminary Estimates of Radiative Transfer Effects on Detached Shock Layers", AIAA Journal, Vol. 2, No. 3, March 1962, pp.494-502.

14) Lyne, J. E., private communication, University of Tennessee, Knoxville, TN, June 1997.

15) Marvin, J. G. and Deiwert, G. S., "Convective Heat Transfer in Planetary Gases", NASA TR R-224, July 1965.

16) Sutton, K. and Graves, R. A., Jr., "A General Stagnation Point Convective Heating Equation for Arbitrary Gas Mixtures", NASA TR R-376, 1971.

17) Tauber, M. E., "A Review of High-Speed Convective Heat Transfer Computation Methods", NASA Technical Paper 2914, July 1989.

18) Tauber, M. E., Yang, L. and Paterson, J., "Flat Surface Heat Transfer Correlations for Martian Atmospheric Entry", Journal of Spacecraft and Rockets, Vol. 30, No. 2, March-April 1993, pp.164-169.

19) Bouslog, S. M., An, M. Y., Hartmann, L. N. and Derry, S. M., "Review of Boundary Layer Transition Flight data on the Space Shuttle Orbiteer", AIAA Paper 91-0741, Jan. 1991.

20) Dhawan, S. and Narasimha, R., "Some Properties of Boundary Layer Flow During the Transition from Laminar to Turbulent Motion", Journal of Fluid Mechanics, Vol.3, Pt.4, Jan. 1958, pp.418-436.

21) Dorrance, W. H., "Viscous Hypersonic Flow", McGraw-Hill Book Co., Inc., New York, N.Y., 1962.

22) Williams, S. D. and Curry, D. M., "Thermal Protection Materials", NASA Reference Publication 1289, Dec. 1992.

23) Lundell, J.H., "Spallation of the Galileo Probe Heat Shield", from "Entry Vehicle Heating and Thermal Protection Systems: Space Shuttle, Solar Starprobe, Jupiter Galileo Probe", edited by P.E. Bauer and H.E. Colicott, Vol. 85 of Progress in Aeronautics and Astronautics, 1983, pp.496-517.

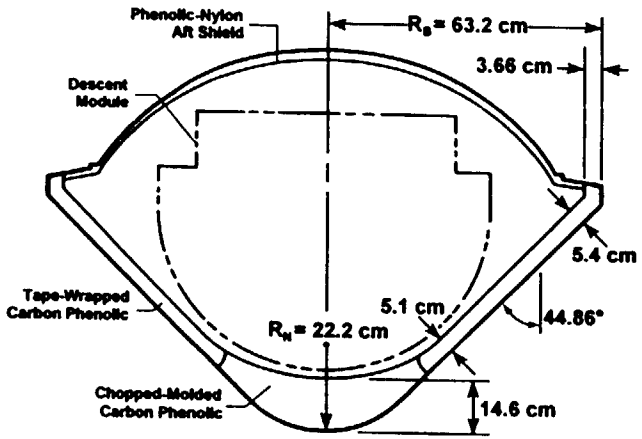

Figure 1. Cross section of Galileo Probe deceleration module.

Fig. 2 Temperatures Behind Normal Shock

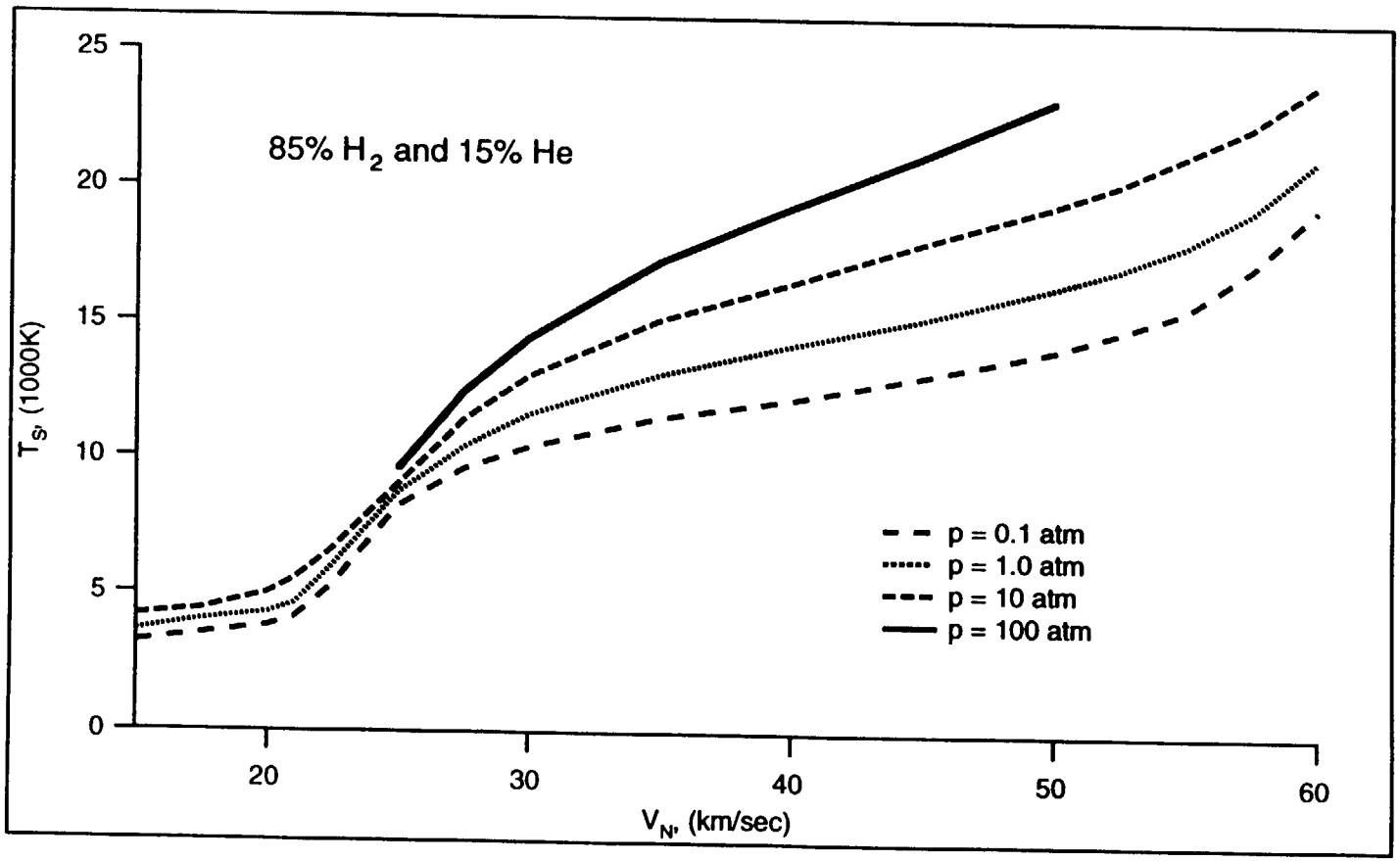

Fig. 3 Radiative Intensity

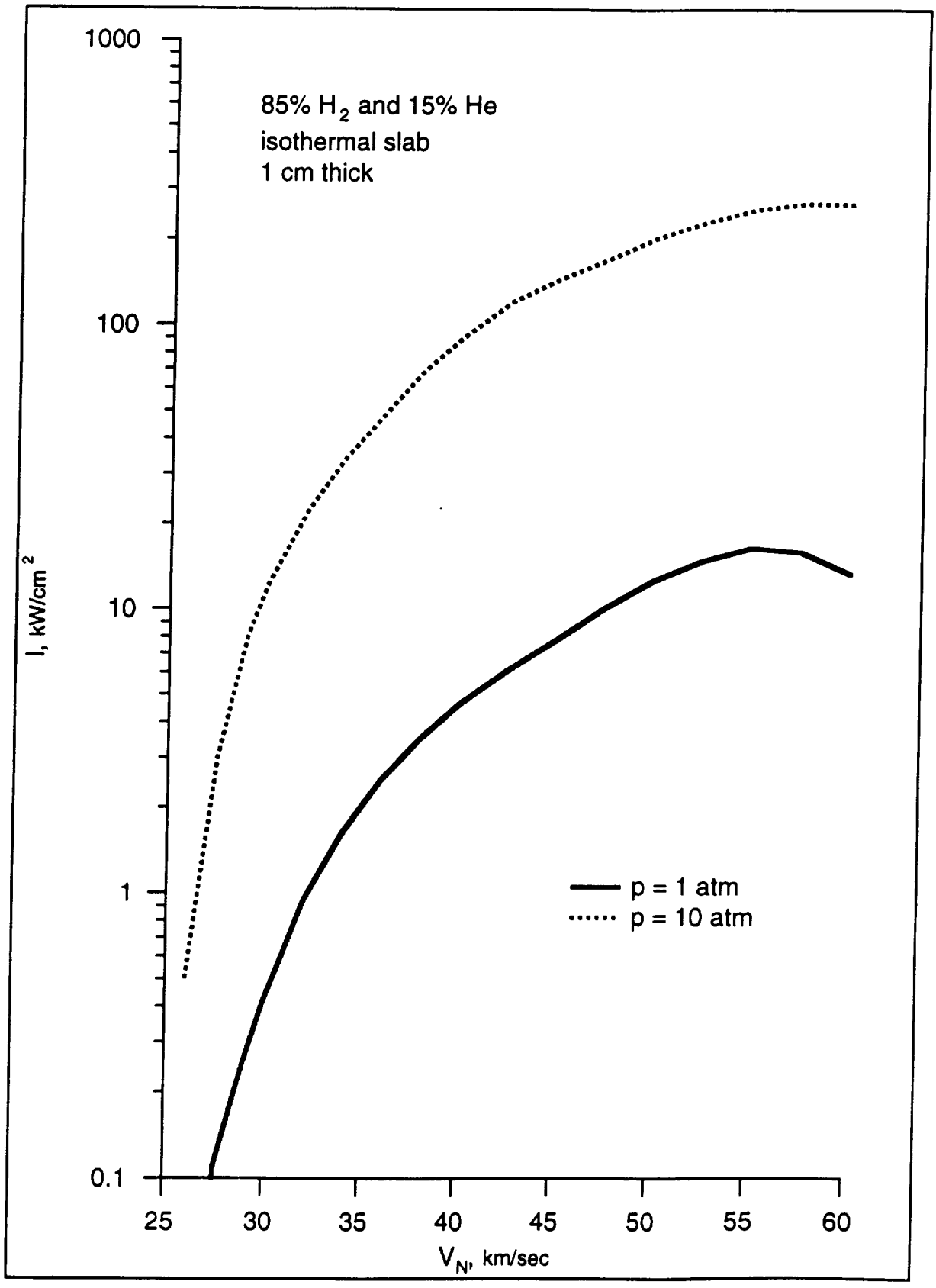

Fig. 4 Calculated Galiloe Probe Trajectory

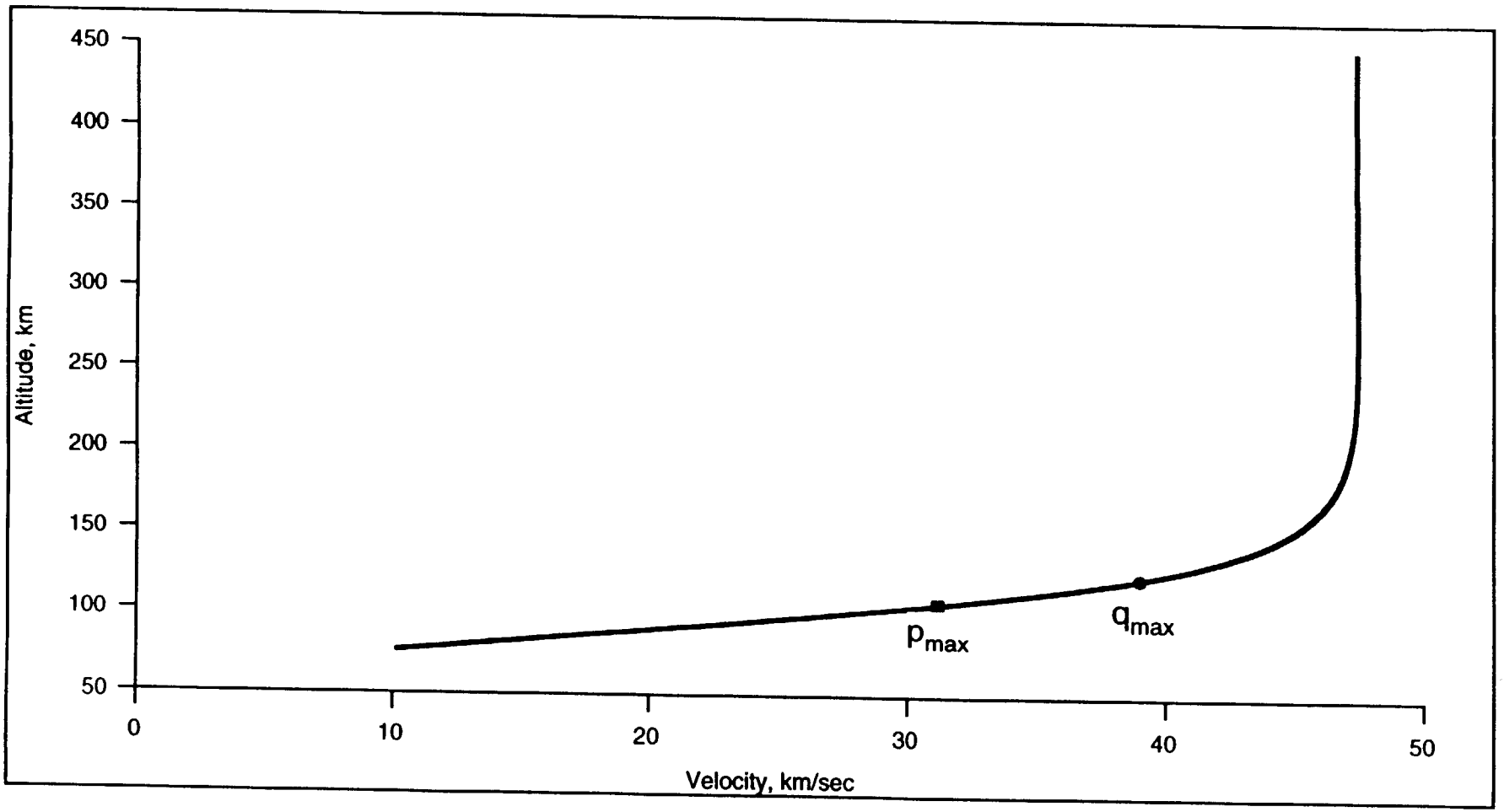

Fig. 5 Calculated Galileo Probe Heating Rate Pulses with Ablation

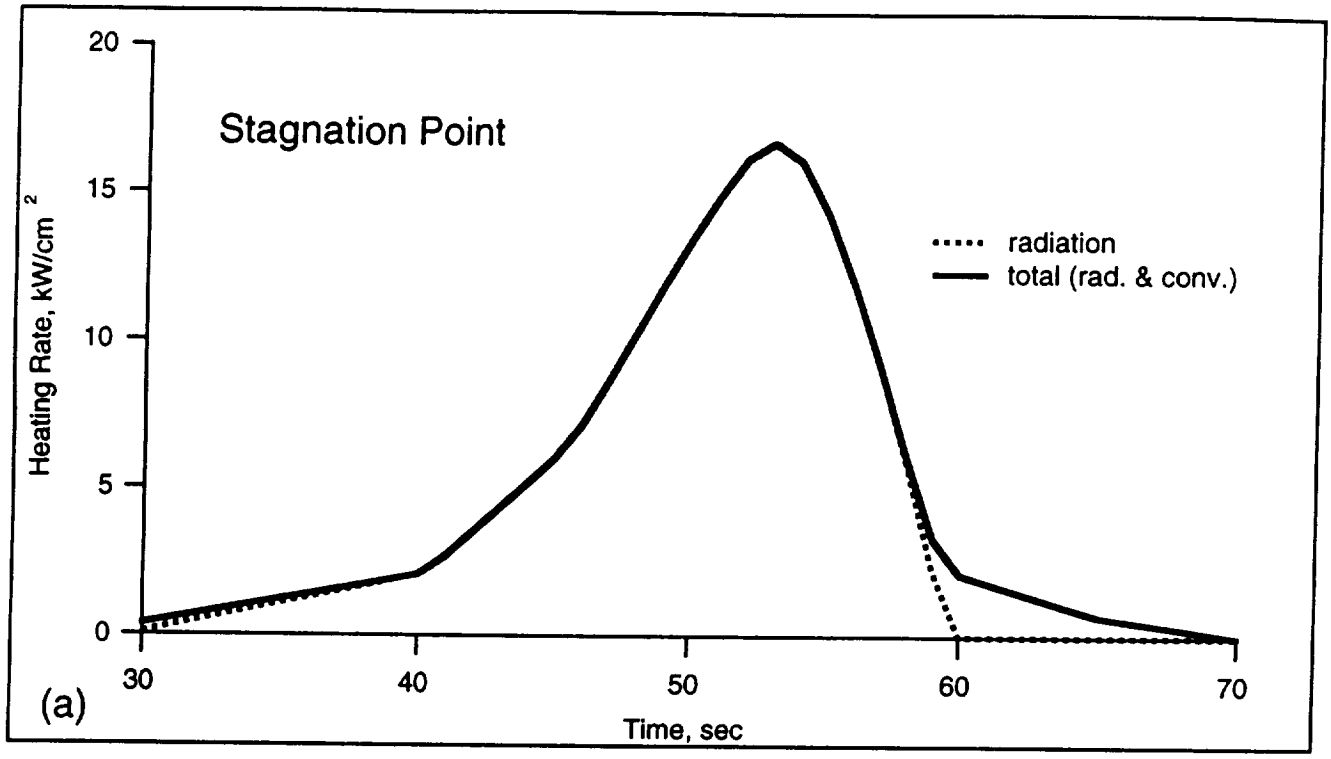

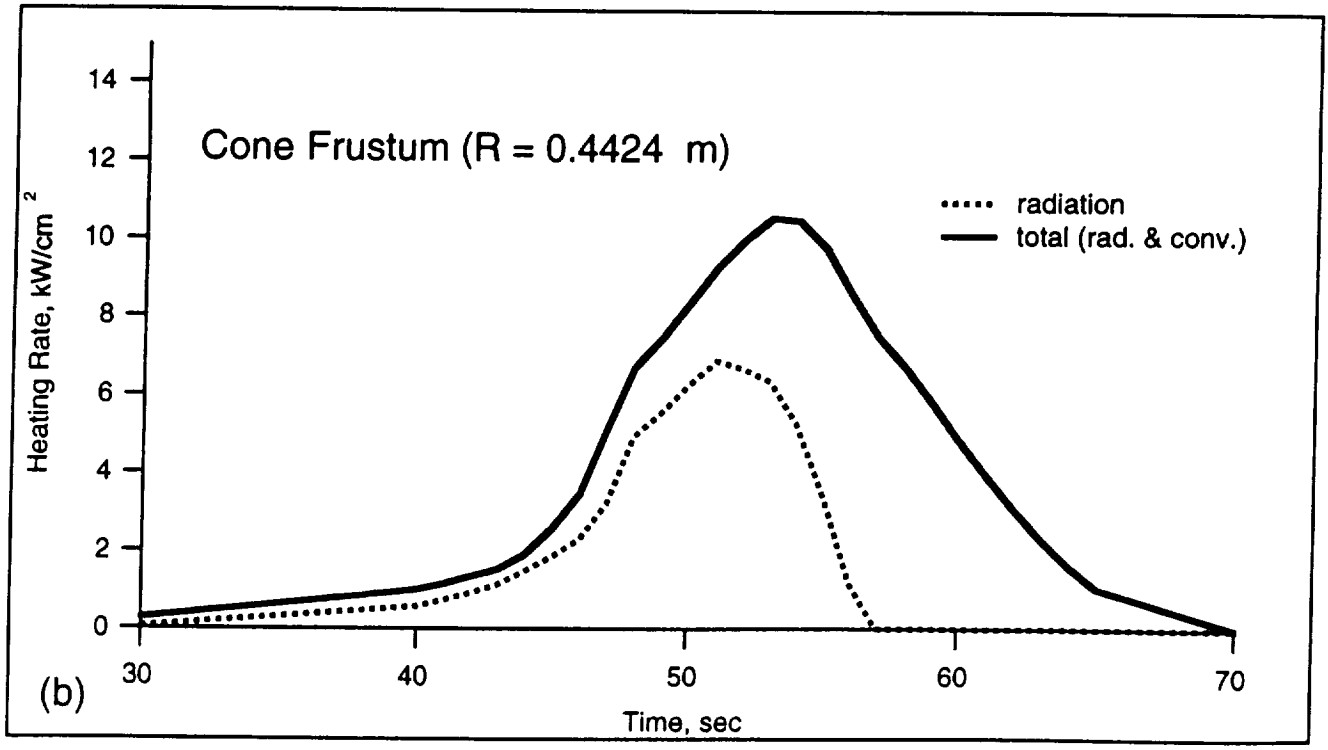

Fig. 6 Calculated Galileo Probe Heating Rate Distributions with Ablation

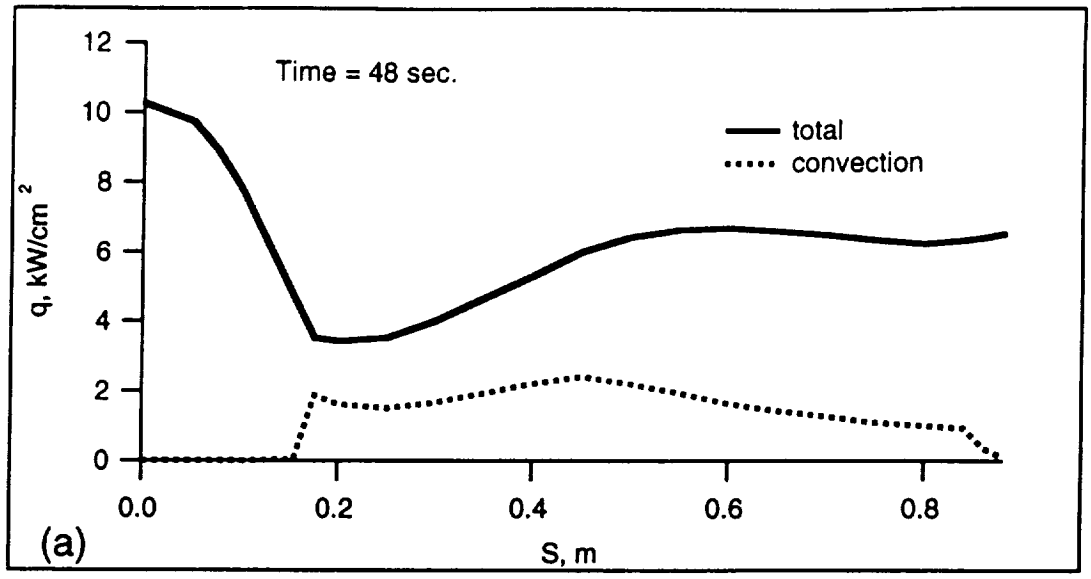

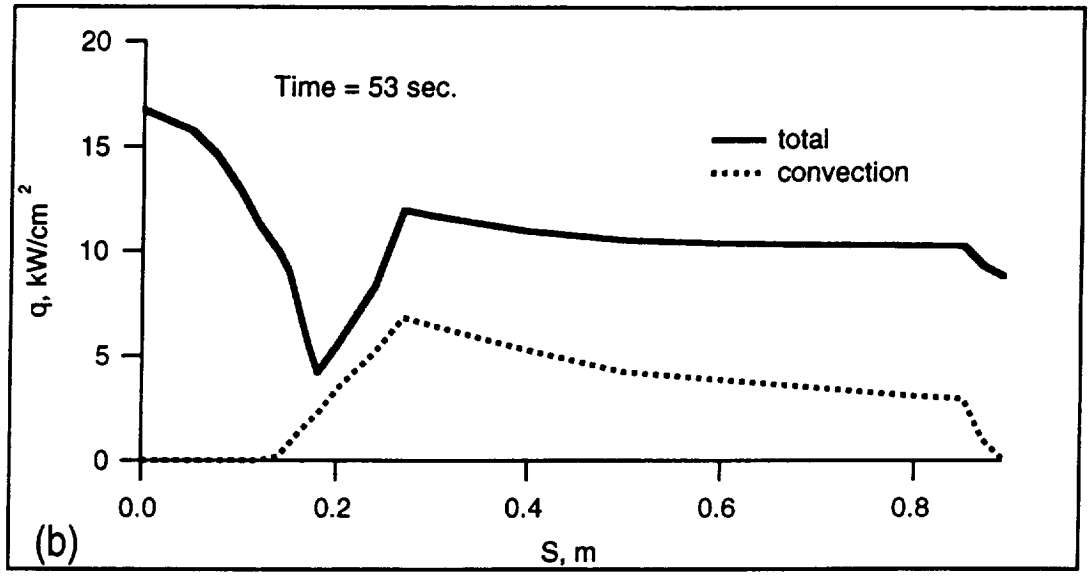

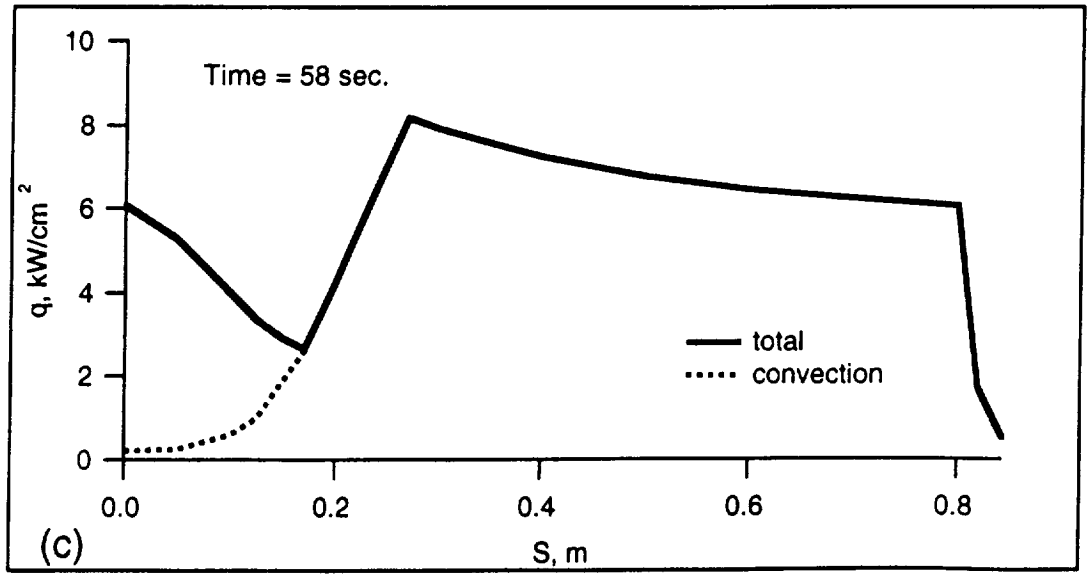

Fig. 7 Surface Recession Comparison with Galileo Probe Data

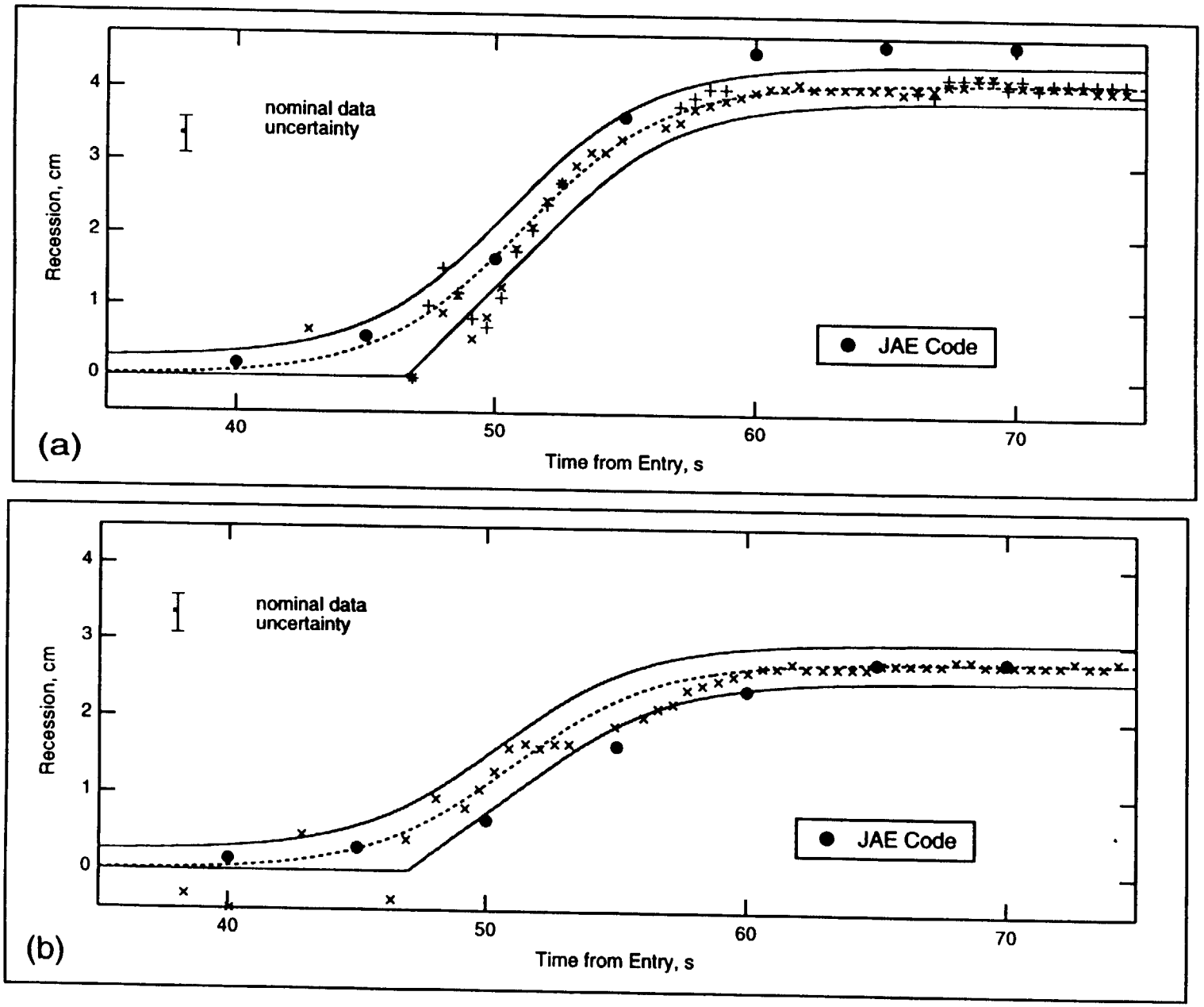

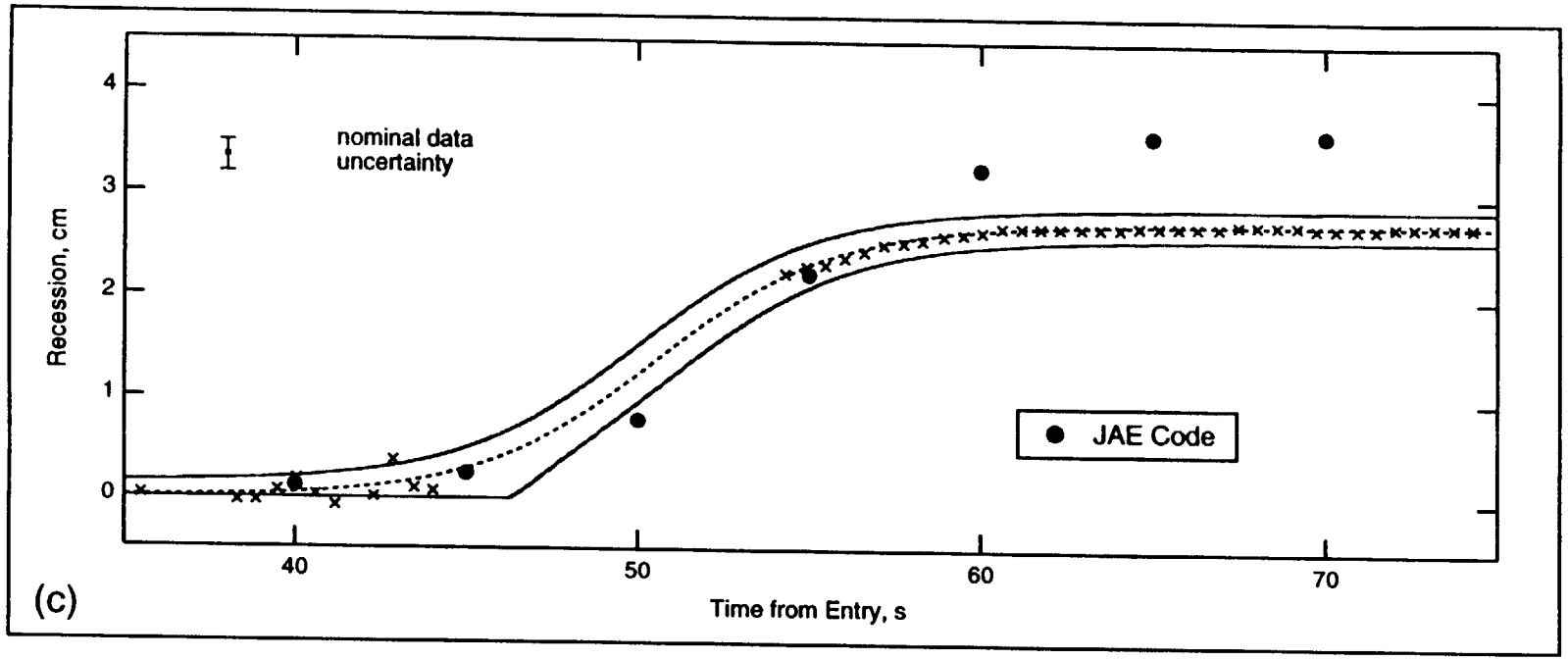
nominal data
uncertainty
JAE Code
Recession, cm
Time from Entry, s
0
1
2
3
4
40
50
60
70
(c)

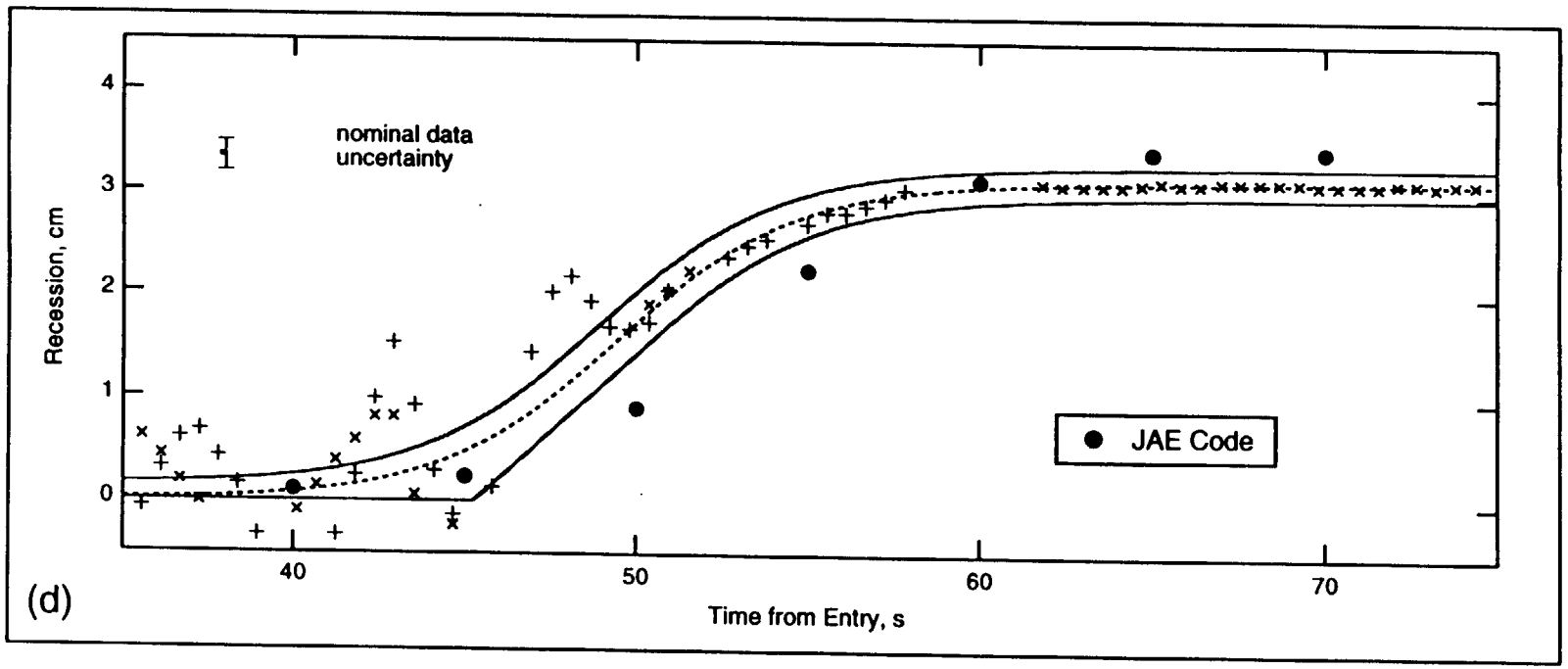
nominal data
uncertainty
JAE Code
Recession, cm
Time from Entry, s
0
1
2
3
4
40
50
60
70
(d)

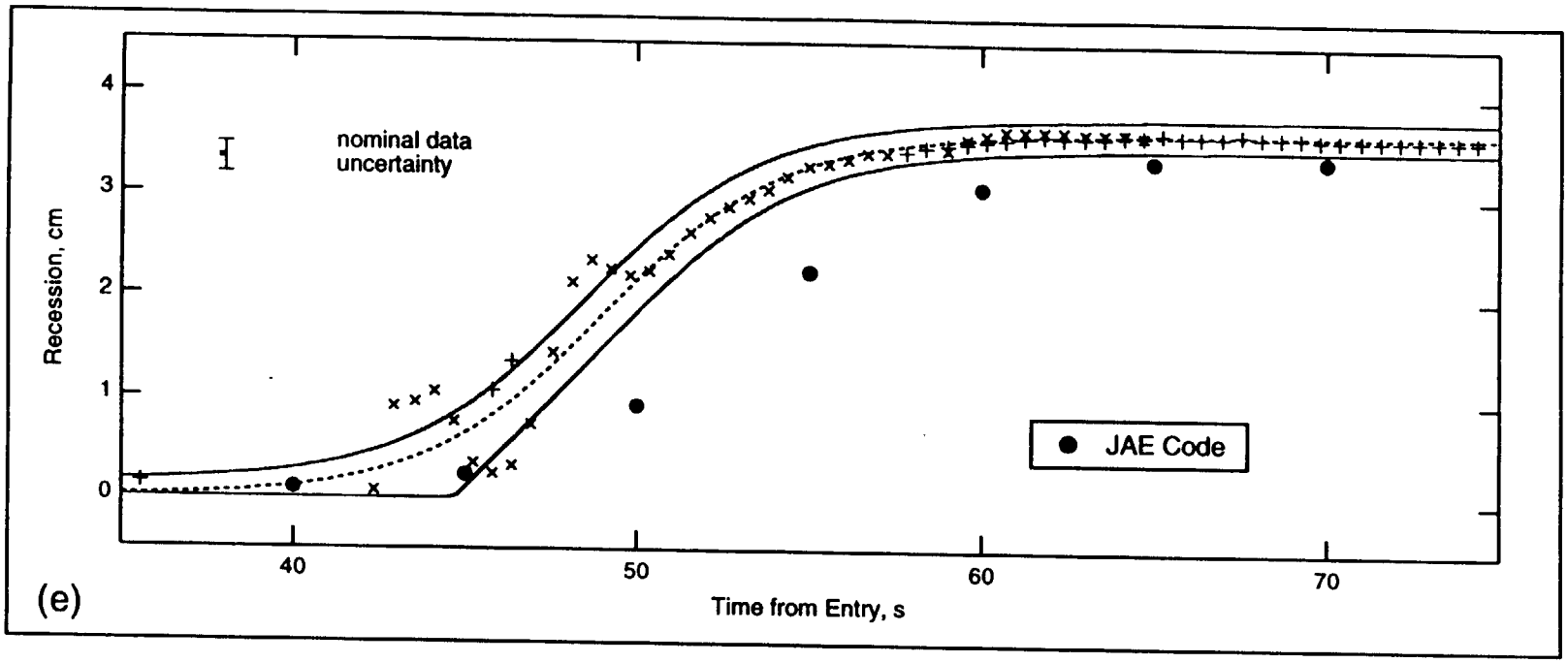
nominal data
uncertainty
JAE Code
Recession, cm
Time from Entry, s
0
1
2
3
4
40
50
60
70
(e)

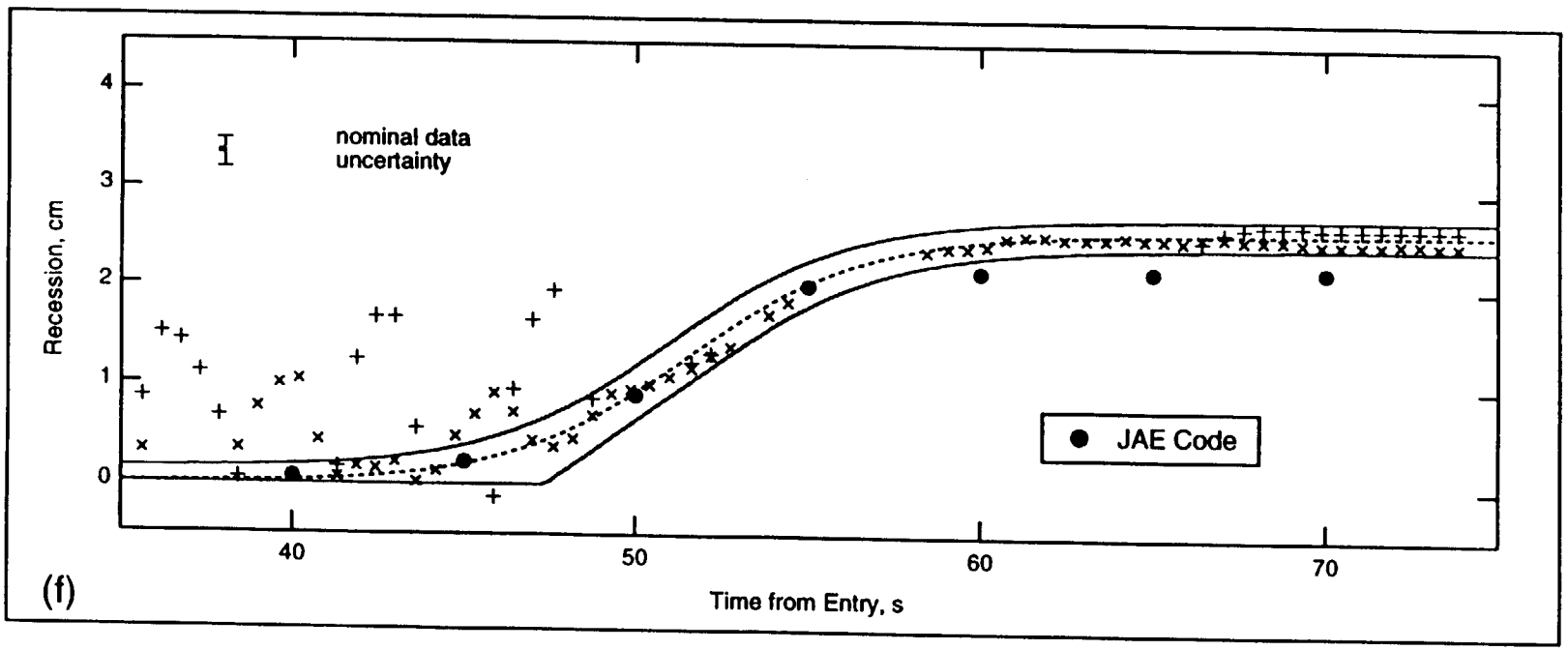
nominal data
uncertainty
JAE Code
Recession, cm
Time from Entry, s
0
1
2
3
4
40
50
60
70
(f)

Fig. 8 Forebody Mass Loss Comparison for Galileo Probe

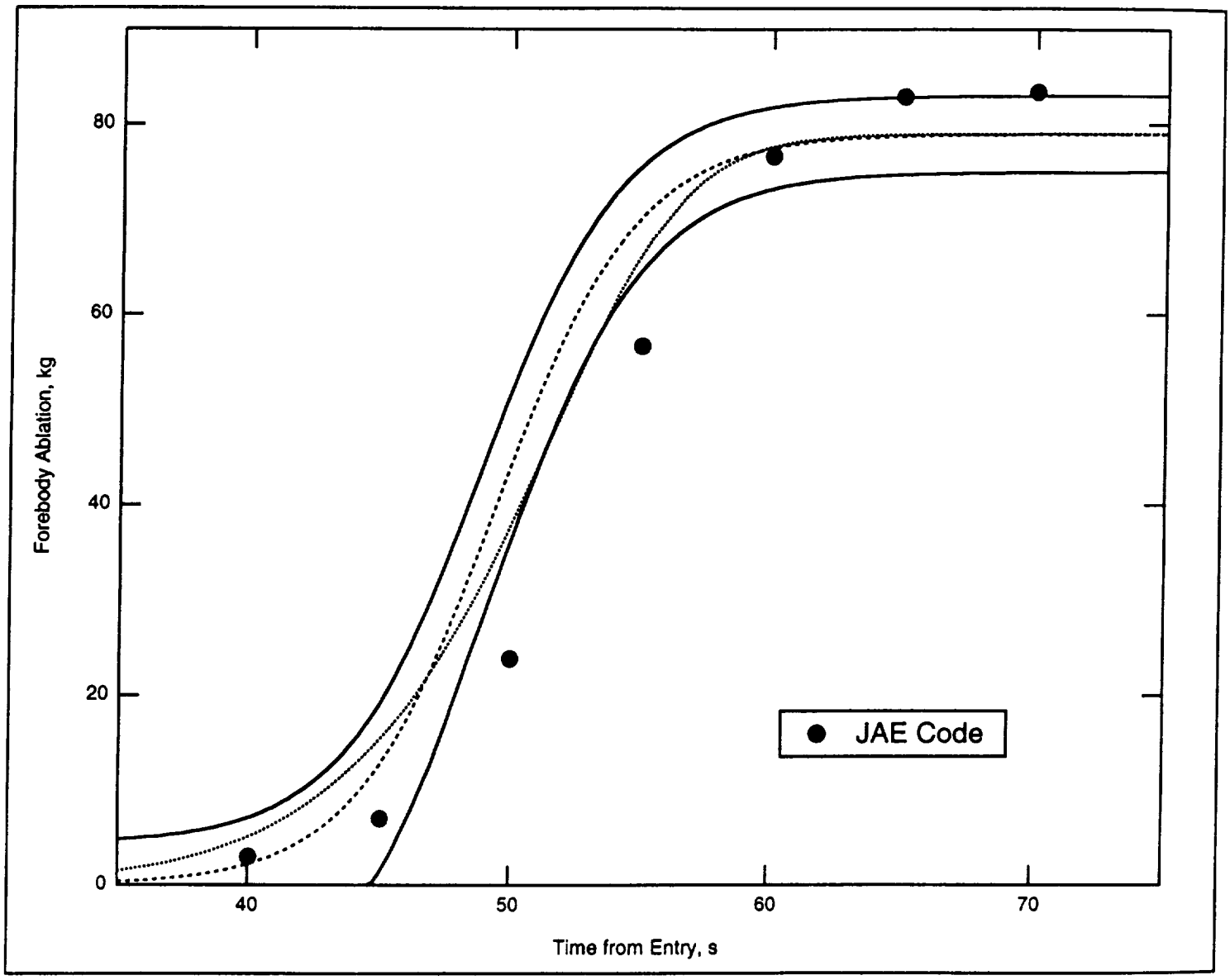

Fig. 9 Calculated Ballistic Coefficient Variation of Galileo Probe